MORPHOLOGIC ANALYSIS OF MARTIAN GULLIES IN FOUR HIGH-NORTHERN LATITUDE CRATERS. R. I. Huang[1] and V. C. Gulick[1,2, 1]Lunar and Planetary Laboratory, University of Arizona, Tucson, AZ, [2]NASA Ames/SETI Institute, Moffett Field, CA.

Introduction: Gullies on Mars are erosional features found on a variety of slopes [1]. They are most commonly located in the Martian mid-latitudes, especially in the southern hemisphere [2]. Their formation mechanism is indeterminate, as Mars' cold, dry modern surface environment encourages "dry" explanations such as dry granular avalanches (e.g., [3]) and CO_2 ice sublimation (e.g., [4, 5]); but some gullies' resemblance to terrestrial analogs implies fluvial formation (e.g., [6]), debris flows (e.g., [7]), or a combination of both (e.g., [8]).

Our study focuses on the morphology of gullies in the high-northern latitudes (>45° N) of Mars, which provides a unique formation environment. Here, the higher surface pressures at lower elevations have the potential to stabilize liquid water [9]. Abundant near-surface ice provides a potential source of water and suppresses the condensation of CO_2 frosts [10]. These factors make the northern lowlands of Mars one of the environments most conducive to fluvial processes under recent Martian climatic conditions.

We are interested in understanding whether the gullies could have formed by fluvial processes in these low elevation environments, or if gullies are influenced more by global climatic conditions. We address these questions by detailed mapping of the gully systems and their local environment at HiRISE resolution. We also analyze the detailed slopes, areas, and volumes of the gully systems using HiRISE Digital Terrain Models (DTMs) to quantify the morphometry of gully morphology in greater detail than more global-scale gully surveys (e.g., [2, 11]).

Methods: Following the methods outlined in [6], we begin by mapping the detailed morphology of the gully systems in ArcGIS Pro using HiRISE and CTX image products (Fig. 1). Using these maps, two-dimensional morphology is quantified with parameters that describe the degree of development for channelized systems such as stream order, stream magnitudes, drainage density, drainage area and channel sinuosity.

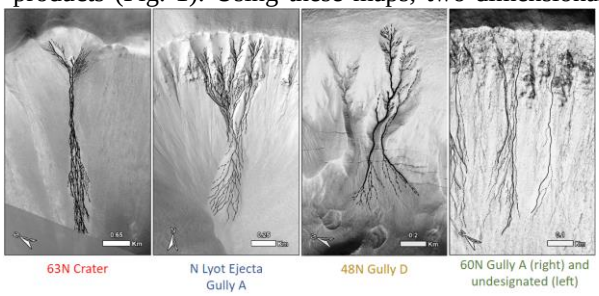

Figure 1: *Drainage maps of a selection of gullies in each study site. All gullies have distinct shapes and channel connections.*

We examined both the normalized- and non-normalized longitudinal profile of each gully system along the CSL (Center Stream Line; the longest and deepest channel in the system), and calculate slopes at different points along the gully profile. In both ArcGIS Pro and ENVI, we also calculate both gully and apron volumes within each gully system (Fig. 2).

TES surface temperature and pressure data and THEMIS temperature data are used to determine present-day volatile stability conditions.

Study Sites: We focused our present analysis on four low-elevation gullied craters in the Martian Northern Hemisphere. These sites were selected based on size and longitudinal distribution in addition to availability of HiRISE DTMs.

Table 1: *Study site locations and crater characteristics*

Crater	Center Lat. [dd]	Center Lon. [dd]	Crater Diam. [km]	Floor Elev. [m]
63N Crater	63.78°	292.3°	16	-5700
N Lyot Ejecta	53.55°	26.31°	4.5	-4600
60N Crater	60.21°	236.2°	3	-3700
48N Crater	48.46°	89.375°	12	-4600

Preliminary Results: Fig. 1 shows gully systems at each site. All gullies formed tributaries in their source regions. 63N had the highest Shreve magnitude of 43 and Strahler order of 4. By contrast, the 60N gullies had the lowest stream orders with an average Shreve magnitude of 6.6 and an average Strahler order of 2.6.

All of the gullies have concave-up normalized center stream profiles, which are consistent with fluvial longitudinal profiles. 48N has the most concave profile (CI ≃ 0.25; more consistent with fluvial erosion) and the 60N gully profiles are nearly straight (CI ≃ 0.04; more consistent with dry flows).

The apron apex slopes of the gullies in 63N, N Lyot Ejecta, and 48N fall below the angle of kinetic friction (<21°; [12]) (average angles of 11.37°, 20.14°, and 11.55° respectively), while those of 60N near the angle of repose (~35°?) with an average apex slope of 32.98°.

Our study gullies had smaller apron volumes when compared to their corresponding gully volumes. During volume analysis, cross-sectional profiles of the gully systems were V-shaped for all our study sites (Fig. 2).

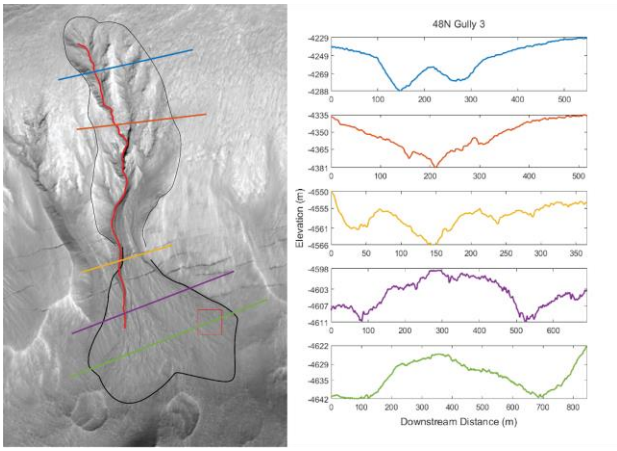

Figure 2*: Plots of cross-sectional profiles (right) against the transect locations along the gully (left).*

TES and THEMIS results show that surface temperatures at the given pressures do not approach CO_2 ice stability, but do approach the stability zone for liquid water (Fig. 3).

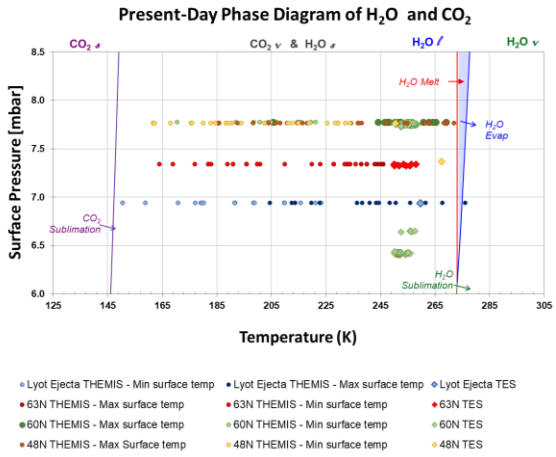

Figure 3*: TES and THEMIS Ts data vs. TES Ps within each study crater. THEMIS Ts are plotted against maximum TES Ps.*

Ongoing Discussion: Based on these results, the formation of the 60N crater gullies is consistent with dry avalanching. The channels in these gullies are poorly networked, formed on higher slopes, and have the straightest longitudinal profiles of our study sites. The sinuous nature of the channels is not congruous with this explanation [13]; but the observed surface temperatures and pressures do not approach the CO_2 ice stability range (Fig. 3). Though bright flows may also imply recent activity, we observed no surface changes throughout HiRISE monitoring.

However, our results for the 63N, N Lyot Ejecta, and 48N craters suggest that these gullies are most consistent with a formation by fluvial processes. These gullies are on low slopes, which would require fluids to emplace material below the angle of kinetic friction [12]. Additionally, their concave profiles and decreased fan volumes suggest that a fluid has eroded the gully and subsequently evaporated or infiltrated from the system, leaving a smaller than expected fan volume. This would not be the case for dry flows. 63N and N Lyot Ejecta crater gullies in particular have high Shreve stream magnitudes, and all gullies erode deeply (>40 m) into bedrock, which implies an extended period of channel erosion and development.

Due to Mars' current surface environment, gullies that appear to be formed by fluvial processes have been attributed to a past, more favorable obliquity [14]. Potential water sources that have been proposed for fluvial gully formation include snowmelt (e.g., [7]), aquifer release (e.g. [2]), and the melting of near-surface ice (e.g., [14, 15]). These processes have different implications for Mars' past environment and climate variability. For example, the gully in 63N has a bright, IRB-blue incised mound within the deepest part of its alcove. If we interpret it as a dust-covered snowpack or ice deposit [15], it could imply melting snow formed the gully channels seasonally, which in turn suggests Mars was cold and wet, rather than warm and wet, at the time of gully formation. 48N crater has concentric crater fill on its floor which limits the length of the gullies despite the craters' size. In this case did gullying take place concurrently with glacial processes? These landform assemblages that differ between gully systems may be diagnostic of variabilities between gully sites during formation. If this is the case, gully formation may also be influenced by processes acting in its local environment.

These preliminary results show the need to analyze gully sites within the context of their surroundings. Fluvially formed gullies may not solely be products of a global favorable climate, but rather the result of local stabilizing factors or microclimates.

References: [1] Malin and Edgett (2000) Science, 288, 2330-2335. [2] Harrison et al. (2015) Icarus, 252, 236-254. [3] Treiman (2003) JGR: Planets, 108, E4. [4] Diniega et al. (2013) Icarus, 225, 526-537. [5] Dundas. et al. (2019) GSL Spec. Pub., 467, 67-94. [6] Gulick et al. (2019) GSL Spec. Pub., 467, 233-265. [7] Hartmann et al. (2003) Icarus, 162, 259-277. [8] Conway et al. (2015) Icarus, 253, 189-204. [9] Haberle et al. (2001) JGR: Planets, 106, 23317-23326. [10] Haberle et al. (2008) Planet. & Space Sci., 56, 251-255. [11] de Haas et al. (2019) GSL Special Pub., 467, 165-186. [12] Kolb et al. (2010) Icarus, 208, 132-142. [13] Conway et al. (2019), GSL Spec. Pub., 467, 7-66. [14] Costard et al. (2001) Science, 295, 110-113. [15] Khuller et al. (2021) JGR: Planets, 126, 2.